Effect of errors in baseline optical properties on accuracy of transabdominal near-infrared spectroscopy in fetal sheep brain during hypoxic stress

Theresa Mawn
University of Pennsylvania
Department of Bioengineering
Philadelphia, Pennsylvania 19104-6100

Shoko Nioka
University of Pennsylvania
Department of Biochemistry and Biophysics
Philadelphia, Pennsylvania 19104-6100

Mark Nijland
Cornell University
Department of Biomedical Sciences
Ithaca, New York 14853-6401

Luke Bloy
Mark A. Elliott
University of Pennsylvania
Department of Radiology
Philadelphia, Pennsylvania 19104-6100

Britton Chance
University of Pennsylvania
Department of Biochemistry and Biophysics
Philadelphia, Pennsylvania 19104-6100

John S. Leigh
University of Pennsylvania
Department of Radiology
Philadelphia, Pennsylvania 19104-6100

Abstract. A continuous-wave (cw) near-infrared spectroscopy (NIRS) instrument has been developed to noninvasively quantify fetal cerebral blood oxygen saturation (StO_2). A linear Green's function formulism was used to analytically solve the photon diffusion equation and extract the time-varying fetal tissue oxy- and deoxy-hemoglobin concentrations from the NIR measurements. Here we explored the accuracy with which this instrument can be expected to perform over a range of fetal hypoxic states. We investigated the dependence of this accuracy on the accuracy of the reference optical properties chosen based on the literature. The fetal oxygenation of a pregnant ewe model was altered via maternal aortic occlusion. The NIR cw instrument was placed on the maternal abdomen directly above the fetal head, continuously acquiring diffuse optical measurements. Blood was sampled periodically from the fetus to obtain fetal arterial saturation (SaO_2) measurements from blood gas analysis. The NIR StO_2 values were compared with the fetal SaO_2 measurements. Variations in the NIR results due to uncertainty in the reference optical properties were relatively small within the fetal SaO_2 range of 30 to 80%. Under hypoxic conditions, however, the variability of the NIR StO_2 calculations with changes in the assumed reference properties became more significant.
[DOI: 10.1117/1.2118730]

Keywords: diffusion theory; photon migration; hemoglobin; saturation.

Paper 04187RR received Sep. 28, 2004; revised manuscript received Apr. 12, 2005 and Jun. 1, 2005; accepted for publication Jun. 3, 2005; published online Nov. 2, 2005.

1 Introduction

The ability to confidently assess fetal oxygenation is of great importance to obstetricians, midwives, and parents. A deficiency of oxygen in fetal blood can lead to permanent brain damage, neurological disorders, or even death.[1,2] Although there are a number of methods currently used to determine fetal health, most are indirect monitors of fetal oxygenation. During times of uncertainty, physicians are forced to decide whether a fetus is in distress and if cesarean delivery is necessary based on the information available to them. Electronic fetal monitors (EFM) are commonly used for fetal heart rate monitoring, the standard for assessing fetal well-being. However, studies have shown that "nonreassuring" fetal heart rate patterns are not always indicative of fetal compromise. In fact, they have been associated with a high rate of false-positive *ante partum* assessment tests.[1–4] Fetal scalp blood sampling (FBS), which offers a measure of fetal pH (an indicator of fetal hypoxia), is invasive and can only provide intermittent information.[2] Transvaginal fetal pulse oximetry is a newer method, which measures fetal arterial saturation by placing an optical sensor on the fetal head or cheek. However, this method can only be used during labor and can be unreliable due to motion and low perfusion.[5]

Transabdominal NIRS offers a noninvasive method to continuously monitor blood oxygen saturation and blood volume, *in utero*. Biological tissue is relatively transparent in the NIR region (600 to 1000 nm), allowing NIR photons to probe deeply before being absorbed or returning to the tissue surface.[6,7] Photons that do not return to the surface are absorbed by various tissue chromophores (e.g., water, hemoglobin, lipids, etc.). In the fetal brain, absorption is primarily due to oxy- and deoxy-hemoglobin (HbO and Hb, respectively).[8] The use of multiple wavelengths and the knowledge of chro-

Address all correspondence to Theresa Mawn, Bioengineering Department, University of Pennsylvania, 422 Curie Boulevard – B1 Stellar Chance Labs, Philadelphia, PA 19104. Tel: 215–898–9327. Fax: 215–573–2113. E-mail: tmawn@seas.upenn.edu

1083-3668/2005/10(6)/064001/8/$22.00 © 2005 SPIE

mophore specific wavelength-dependent molar extinction coefficients allows for the determination of these chromophore concentrations.[9]

Several developments have been made to improve the ability of NIRS to offer more accurate quantitative information. Continuous-wave (cw) instruments require *a priori* knowledge of the baseline optical properties, or differential pathlength factor (DPF), in order to map amplitude measurements to absolute chromophore concentrations. The DPF is the absolute pathlength (dependent on the tissue optical properties, tissue geometry, and boundary conditions) divided by the optode spacing on the surface. Several investigators have measured this parameter for various tissue types. However, variability in baseline blood volume and saturation among individuals yields uncertain results.[10–12] Frequency-domain (FD) methods[13] and time-resolved spectroscopy (TRS)[14,15] acquire absorption and scattering properties by fitting phase and temporal measurements, respectively, to theoretical models based on the diffusion equation.[16] The quantitative accuracy of the FD and TRS methods, therefore, relies on the theoretical model used to estimate the baseline optical properties. Accurately quantifying cerebral blood saturation in adults, neonates,[17] or the fetus (transabdominally) is challenging, regardless of the NIR instrumentation used.

Previous studies have demonstrated, through simulations,[18–22] phantom models,[23] and *in vivo* experiments,[22,24] the feasibility of detecting NIR photons that have penetrated an underlying fetal layer, centimeters deep. There has been a discussion among investigators as to which photon diffusion model most accurately describes photon propagation through a two-layer model,[11,12,14,16,22] such as that described here. In a study by Choe et al.[25] a multiseparation, frequency-domain NIR instrument was employed to obtain cerebral blood saturation measurements of an ovine fetus at various stages of hypoxia, *in utero*. A numerical solution was used to solve the diffusion equation for the two-layer model. Several assumptions were made about the baseline optical properties of both the maternal and fetal layers, in order to quantify NIR blood saturation measurements.

The goal of this study is to demonstrate the feasibility of quantifying NIR transabdominal fetal blood saturation measurements, assuming there is uncertainty in the chosen baseline optical properties, and to investigate the error propagation due to incorrect baseline assumptions. A pregnant ewe model was manipulated to allow for a controlled method of altering the fetal blood saturation. A three-wavelength (730, 805, and 850 nm), single-separation, cw NIR instrument was employed to make transabdominal measurements of fetal oxygenation changes. The following sections describe in more detail the experimental protocol and instrumentation that was implemented. Next, the analytical solution used to estimate photon diffusion in this two-layer model is discussed thoroughly. Finally, the results present the extent of error propagation in the NIR StO_2 calculations as several baseline optical properties are varied, specifically, the baseline fetal and maternal absorption coefficients, and the global reduced scattering coefficient.

2 Materials and Methods

2.1 *Animal Preparation*

This animal study followed the National Institute of Health guidelines of the Institutional Animal Care and Use Committee at Cornell University, Ithaca, New York. This experiment was performed using a pregnant ewe model at a gestational age between 130 to 150 days (normal term 148 days). The dam was anaesthetized with halothane and mechanically ventilated with 50% N_2O and 1.25% isoflurane. A midline abdominal incision exposed the uterus and a hysterotomy was performed to expose the fetal head.[26] The fetal head was exteriorized from the amniotic sac. The left fetal brachial artery was catheterized for obtaining arterial blood samples and the right brachial artery was catheterized to monitor fetal blood pressure. The ears were sutured to the maternal abdomen such that the fetal head was directly under the maternal tissue, measured to be approximately 0.5 cm thick. This procedure was done to eliminate the effect of amniotic fluid on the NIR measurements. A catheter was inserted through the maternal femoral artery with a balloon for aortic occlusion anterior to the common iliac artery. Occlusion was performed in a stepwise manner by incrementally filling the balloon with saline. This procedure induces fetal hypoxia by gradually limiting the amount of blood flow to the uterus and fetus, while not significantly affecting maternal oxygenation. A pulse oximeter was placed on the maternal ear to continuously measure arterial saturation and monitor maternal stability. Arterial blood samples were taken from the fetal brachial artery throughout the experiment. The fetal SaO_2, Hb, pO2, pCO2, and pH values were measured by blood gas analysis using an OSM3 hemoximeter (Radiometer, Copenhagen) and an ABL605 blood gas analyzer (Radiometer, Copenhagen).

2.2 *Instrumentation*

The cw NIR spectroscopy probe consisted of one source position and one detector position. The optode separation was determined using a fast Fourier transform analysis of the signal component fluctuating at the fetal heart rate, which was simultaneously detected by an ultrasound fetal heart monitor placed on the maternal abdomen (Hewlett Packard m300). The highest signal-to-noise ratio ($\sim$8) was found at an optode separation of 7 cm. The optical probe was placed on the maternal abdomen, such that the source and detector straddled the region above the fetal head. Three LEDs were implemented at 730, 805, and 850 nm (Epitex, L735/805/850—40B32) and time-multiplexed. The intensities at each wavelength were detected by a photomultiplier (Hamamatsu Photosensor Module H6780). The signals were then filtered and sampled by an analog-to-digital converter (Real Time Devices, Inc. ADA2110). The data points were averaged at 85 Hz by the data acquisition software and saved for postprocessing.

2.3 *Data Analysis*

2.3.1 *The model*

The diffusion approximation of the radiative transport equation is the analytical model widely used to analyze photon migration in highly diffusive media. The diffusion approximation is based on the assumption that light propagating in

highly scattering media is close to isotropic due to multiple scattering events. A large number of medical applications involving NIR spectroscopy or optical imaging have taken advantage of these approximations and have employed the diffusion equation to optically characterize and monitor the health status of biological tissue.[27]

In the diffusion approximation, the diffuse intensity moving in direction $\hat{\mathbf{s}}$ at position $\mathbf{r}$ and at time t may be expanded in spherical harmonics and expressed as the sum of two terms, one isotropic term proportional to the fluence rate and one term proportional to the diffused radiation flux:[28]

$$I(\mathbf{r},\hat{\mathbf{s}},t)=\frac{1}{4\pi}cu(\mathbf{r},t)-\frac{3}{4\pi}D\hat{\mathbf{s}}\cdot\nabla u(\mathbf{r},t). \tag{1}$$

Here, $u(\mathbf{r},t)$ is the energy density, and D [cm] is the photon diffusion coefficient defined as $1/(3\mu_s')$, where μ_s' [cm^{-1}] is the reduced scattering coefficient of the medium. In the diffusion approximation, the directional flux is negligible compared to the isotropic term and can be omitted.[29,30] The detected signal is, therefore, considered approximately proportional to the energy density $u(\mathbf{r},t)$.

The diffusion equation follows from this approximation and can be derived as

$$\frac{\partial u(\mathbf{r},t)}{\partial t}=cD\nabla^2u(\mathbf{r},t)-c\mu_a u(\mathbf{r},t)+S(\mathbf{r},t), \tag{2}$$

where μ_a [cm^{-1}] is the absorption coefficient, c is the speed of light in the medium, and $S(\mathbf{r},t)$ is the source. The Green's function solution to the diffusion equation for an isotropic cw point light source in an infinite homogeneous medium is

$$G_0(\mathbf{r},\mathbf{r_s})=\frac{1}{4\pi cD}\frac{\exp(-(3\mu_s'\mu_a)^{-1/2}|\mathbf{r}-\mathbf{r_s}|)}{|\mathbf{r}-\mathbf{r_s}|}, \tag{3}$$

where $|\mathbf{r}-\mathbf{r_s}|$ is the distance from $\mathbf{r}$ to the source.

The infinite medium solution to the diffusion equation, however, does not accurately describe a situation in which the source and detector are placed on the surface of the tissue being investigated, as was done in this study. The necessary boundary condition must be implemented that accounts for the internal reflection encountered in a semi-infinite medium or half-space geometry. The extrapolated boundary approach was employed using the dipole method,[31] wherein the fluence is nonzero on the boundary and set equal to zero at an extrapolated boundary located a distance z_b outside the medium. In this dipole configuration a real light source is positioned beneath the surface at a distance $z_s=1/\mu_s'$, and a virtual image source is positioned directly above the surface at a distance $z_i=z_s+2z_b$. The effective diffuse Frenel reflectance for a relative index of refraction of $n=1.40$ (commonly assumed for air-tissue boundaries) was calculated as $R_{eff}=0.493$ according to Haskell et al.[30] The extrapolated boundary z_b was then calculated as a function of the effective Fresnel reflectance such that

$$z_b=\frac{1+R_{eff}}{1-R_{eff}}2D. \tag{4}$$

This boundary condition was found by Kienle and Patterson[32] to accurately resolve μ_s' and μ_a from data generated with Monte Carlo to within 10% and 15%, respectively.

The resulting Green's function solution to the diffusion equation for a semi-infinite homogeneous medium is

$$G_0(\mathbf{r},\mathbf{r_s})=\frac{1}{4\pi cD}\left\{\frac{\exp[-(3\mu_s'\mu_a)^{-1/2}|\mathbf{r}-\mathbf{r_s}|]}{|\mathbf{r}-\mathbf{r_s}|}-\frac{\exp[-(3\mu_s'\mu_a)^{-1/2}|\mathbf{r}-\mathbf{r}_i|]}{|\mathbf{r}-\mathbf{r}_i|}\right\}, \tag{5}$$

where $|\mathbf{r}-\mathbf{r}_i|$ is the distance from $\mathbf{r}$ to the virtual image source.

The volume being investigated in this study, however, was not an ideal homogeneous half-space. Rather it consisted of two layers, an upper maternal layer and a lower fetal layer. Although, it was assumed that the tissue scattering coefficient μ_s' was uniform over both layers,[22,25] each layer could be characterized by its intrinsic absorption coefficient, which is a function of tissue blood volume and tissue blood oxygen saturation. In order to utilize the homogeneous Green's function, a global absorption coefficient μ_{a0}, taking into effect both the maternal and fetal baseline absorption coefficients, was used to represent a homogeneous absorption coefficient. It was assumed that fluctuations in absorption $\alpha(\mathbf{r},t)$ [nsec^{-1}] occurred within and uniformly over an entire layer and were defined with reference to μ_{a0}, such that

$$\alpha(\mathbf{r},t)=[\mu_a(\mathbf{r},t)-\mu_{a0}]\cdot c, \tag{6}$$

where $\mu_a(\mathbf{r},t)$ is the variable absorption coefficient at position $\mathbf{r}$ and at time t.

Therefore, measured changes in intensity were attributed to a fluctuating absorption coefficient in either one or both of the layers. The intensity measured by the detector was considered proportional to the energy density $u_\lambda(t)=u_\lambda(\mathbf{r_d},t)$, which can be approximated as a linear function as described by:[33]

$$u_\lambda(t)=u_{0\lambda}\exp\left[-\int \mathrm{d}^3\mathrm{r}\Gamma_\lambda(\mathbf{r})\alpha_\lambda(\mathbf{r},t)\right]. \tag{7}$$

The weighting function $\Gamma_\lambda(\mathbf{r})$ was computed at each voxel in the entire volume, such that

$$\Gamma_\lambda(\mathbf{r})=\frac{G_{0\lambda}(\mathbf{r},\mathbf{r_s})G_{0\lambda}(\mathbf{r},\mathbf{r_d})}{G_{0\lambda}(\mathbf{r_d},\mathbf{r_s})}. \tag{8}$$

The expression $u_{0\lambda}$ in Eq. (7) represents the energy density propagating between the single source-detector pair in the absence of inhomogeneous absorption and can therefore be described by $G_{0\lambda}$, such that

Table 1 Summary of assumed baseline parameters.

Parameters	Maternal	Fetal
tHb (μM)	60–200, best fit: 189	40–80 best fit: 40
StO_2 (%)	60–90, best fit: 60	56.5[b]
μ_s'(805 nm) (cm^{-1})	5–10[a] best fit: 6	

[a]The Mie scattering formula $\mu_s'(\lambda)=A\lambda^{-b}$ was used to determine the scattering coefficient at 730 nm and 850 nm, where $b=0.5$ (Choe et al.[25,37]).
[b]The baseline fetal StO_2 parameter was assumed equal to the initial fetal SaO_2 reading measured by blood gas analysis.

$$u_{0\lambda}=\int \mathrm{d}^3\mathrm{r}_s G_{0\lambda}(\mathbf{r_d},\mathbf{r_s})S(\mathbf{r_s})=S_0 G_{0\lambda}(\mathbf{r_d},\mathbf{r_s}), \tag{9}$$

where S_0 represents the source power density, which in the case of this experiment was continuous wave ($\omega=0$).

The measured energy density, proportional to energy density, fluctuated as we altered the fetal oxygenation. The NIR measurements were first smoothed with a boxcar average of 500 points, corresponding to a 0.17-Hz low-pass filter. This effectively removed arterial and respiratory fluctuations present in the data.

The baseline energy density $u_\lambda(t=0)$ was assumed equal to the mean of the first 20 samples (approximately 2 min). The natural logarithm of the transmission coefficient $T(t)=u_\lambda(t)/u_\lambda(t=0)$ is then expressed as

$$-\ln \mathrm{T}(t)=\int \mathrm{d}^3\mathrm{r}\Gamma_\lambda(\mathbf{r})\alpha_\lambda(\mathbf{r},t)-\int \mathrm{d}^3\mathrm{r}\Gamma_\lambda(\mathbf{r})\alpha_\lambda(\mathbf{r},0), \tag{10}$$

which can be further decomposed into two spatially resolved compartments,

$$-\ln \mathrm{T}(t)=\int_{\mathrm{M}} \mathrm{d}^3\mathrm{r}\Gamma_\lambda(\mathbf{r})[\alpha_\lambda(\mathbf{r},t)-\alpha_\lambda(\mathbf{r},0)]+\int_{\mathrm{F}} \mathrm{d}^3\mathrm{r}\Gamma_\lambda(\mathbf{r}) \times[\alpha_\lambda(\mathbf{r},t)-\alpha_\lambda(\mathbf{r},0)], \tag{11}$$

where the subscripts M and F represent the integral over voxel locations inside the maternal and fetal layers.

In this experiment, it was assumed that the maternal absorption coefficient remains stable and that the fetal layer was the sole contributor to any absorption changes observed in the data. This assumption reduces Eq. (6) to

$$-\ln \mathrm{T}(t)=\int_{\mathrm{F}} \mathrm{d}^3\mathrm{r}\Gamma_\lambda(\mathbf{r})[\mu_{a\lambda}(\mathbf{r},t)-\mu_{a\lambda}(\mathbf{r},0)]\cdot c. \tag{12}$$

It was further assumed that these absorption fluctuations occurred homogeneously over the entire fetal layer, which removes the position dependence from the fetal absorption coefficient and results in a simplified expression for the data:

$$-\ln \mathrm{T}(t)=\alpha_{\lambda F}(t)\int_{\mathrm{F}} \mathrm{d}^3\mathrm{r}\Gamma_\lambda(\mathbf{r}). \tag{13}$$

Here, the integral of Γ_λ [nsec/cm^3] over the fetal layer is essentially the partial differential pathlength (PDP).[34]

A linear least-squares fit of *a priori* spectral information to the data in Eq. (8) was used to calculate the chromophore concentration changes [$\Delta\mathrm{HbO}(t)$ and $\Delta\mathrm{Hb}(t)$] directly. The absolute fetal chromophore concentrations were calculated as follows: $\mathrm{HbO}(t)=\mathrm{HbO}_0+\Delta\mathrm{HbO}(t)$ and $\mathrm{Hb}(t)=\mathrm{Hb}_0+\Delta\mathrm{Hb}(t)$. The initial fetal hemoglobin concentrations HbO_0 and Hb_0 were calculated from assumed fetal tissue blood volume (tHb) and fetal StO_2 at baseline (Table 1). The fetal StO_2 at each time point was then calculated simply as

$$\mathrm{StO}_2(t)=\frac{\mathrm{HbO}(t)}{\mathrm{HbO}(t)+\mathrm{Hb}(t)}. \tag{14}$$

2.3.2 *Baseline optical properties*

The measured chromophore concentration changes are essentially difference measurements from a known reference (baseline) point. Therefore, a NIR StO_2 monitor must take an initial measurement during a stable, usually normoxic, state, during which the baseline absorption and scattering properties can be either measured (e.g., via FD or TRS methods) or safely assumed. The confidence of the NIR StO_2 measurements, thus, relies heavily on the confidence of the chosen baseline properties.

In this study, several baseline parameters were assumed in order to quantify the fetal chromophore concentration fluctuations measured in the data. These parameters were chosen based on values found in the literature[15,22,25,35–38] and are described in Table 1. The maternal tHb, fetal tHb, maternal StO_2, and the global $\mu_s'(\lambda)$ were varied over a range of values, since the literature indicates some intersubject variability. The error propagation due to uncertainty in these baseline parameters was analyzed. The best-fit baseline parameters were determined, using a downhill simplex method,[39] by fitting the calculated fetal StO_2 values to the measured fetal SaO_2 values (Table 1).

The baseline fetal StO_2 was not varied; it was assumed equal to the initial SaO_2 reading taken from blood gas analysis. In this experiment, the fetal StO_2 was expected to remain in close approximation to the fetal SaO_2. This assumption was founded on data published by Choe et al.,[25] in which fetal SaO_2 and local venous saturation (SvO_2) values were often close, if not overlapping, for normoxic and a range of hypoxic states. Generally, StO_2 is modeled as a weighted average of SaO_2 and SvO_2. However, the exact contributions in a subject are unknown and studies have demonstrated that they may not be fixed at all stages of hypoxia.[40] Therefore, there may be some error due to correlating quantified NIR StO_2 values to SaO_2 values, especially at low saturations (severe fetal hypoxia). However, in this study, this source of error has not been investigated; instead, the focus remains on the errors due to other baseline assumptions commonly made in quantifying tissue blood saturation.

The global baseline absorption coefficient $\mu_{a0}(\lambda)$ was calculated as a weighted combination of the maternal baseline

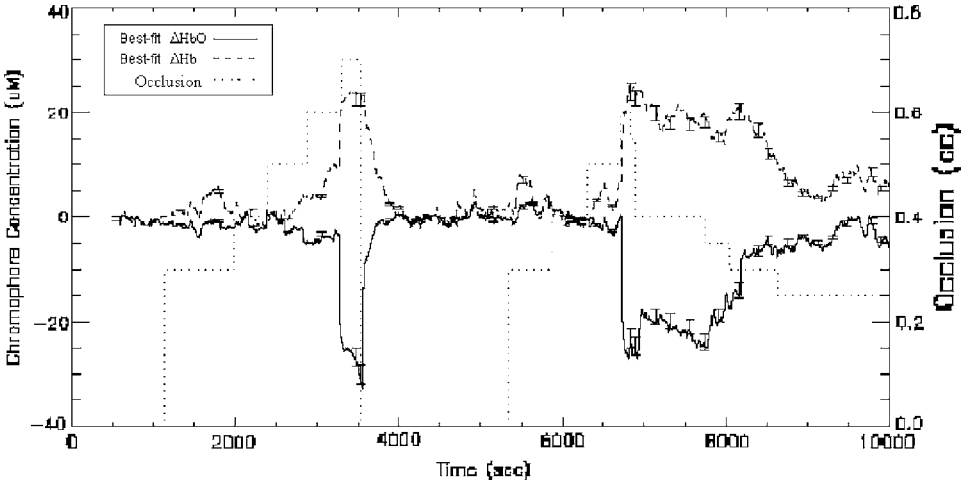

Fig. 1 Fetal hemodynamic response due to occlusion. The solid line represents the average change in [HbO] over the course of the experiment and the dashed line represents the average change in [Hb] over time. The dotted line represents the volume of occlusion by filling a catheterized balloon with saline. The error bars represent the maximum variations in the calculated results as all of the parameters in Table 1 were altered simultaneously.

absorption coefficient $\mu_{a0\mathrm{M}}(\lambda)$ and the fetal baseline absorption coefficient $\mu_{a0\mathrm{F}}(\lambda)$. A wavelength-dependent background term $\mu_a^{\mathrm{bg}}(\lambda)$ representing fat and water[40] was included in the absorption coefficient for each respective layer, such that $\mu_{a0\mathrm{M,F}}(\lambda)=\mu_{a0\mathrm{M,F}}^{\mathrm{Hb}}(\lambda)+\mu_a^{\mathrm{bg}}(\lambda)$. Since the extinction coefficients for fat and water are very similar and the concentration of fat is much less than that of water, $\mu_a^{\mathrm{bg}}(\lambda)=0.9\mu_a^{\mathrm{H_2O}}(\lambda)$. The errors due to the uncertainty in this background term were not considered in this study.

The simplex routine assumed a 1:1 contribution ratio for the maternal and fetal absorption coefficients (a weight of 0.5 for each layer) in the determination of the best-fit baseline parameters. After the best-fit baseline values are chosen, the weight $w_{\mathrm{M,F}}^k(\lambda)$ of each layer absorption coefficient was optimized using a least-mean-square algorithm, iterated over k. The new weights were calculated based on the percent signal contributed from each layer,

$$w_{\mathrm{F}}^k(\lambda)=\frac{\int_{\mathrm{F}}\mathrm{d}^3\mathrm{r}\Gamma_\lambda^k(\mathbf{r})}{\int\mathrm{d}^3\mathrm{r}\Gamma_\lambda^k(\mathbf{r})}, \tag{15}$$

$$w_{\mathrm{M}}^k(\lambda)=1-w_{\mathrm{F}}^k(\lambda). \tag{16}$$

The new global baseline absorption coefficient $\mu_{a0}^k(\lambda)$ was updated such that

$$\mu_{a0}^k(\lambda)=w_{\mathrm{M}}^k(\lambda)\mu_{a0\mathrm{M}}(\lambda)+w_{\mathrm{F}}^k(\lambda)\mu_{a0\mathrm{F}}(\lambda), \tag{17}$$

and the change in squared error $(e^2)^k$ was calculated:

$$(e^2)^k=[\mu_{a0}^k(\lambda)-\mu_{a0}^{k-1}(\lambda)]^2. \tag{18}$$

The absorption coefficient weights were optimized when $(e^2)^k$ was minimized.

3 Results and Discussion

3.1 *Hemodynamic Response in the Fetus Due to Occlusion*

Rather than inflating the catheterized balloon with air, the balloon was incrementally filled with saline in order to observe a more gradual change in fetal chromophore concentrations. The balloon was filled in a step-wise manner, 0.1 cm^3 at a time, as arterial blood samples were taken from the fetus and the fetal SaO_2 values were noted. When fetal SaO_2 values reached a dangerous low, near 20%, the balloon was drained of saline to allow for fetal recovery. The changes in [Hb] and [HbO], calculated from the recorded NIR data, are shown in Fig. 1.

The fetus endured two trials of induced hypoxia and recovery. In the first trial, at 0.3 cm^3 of occlusion, a slight jump in fetal $\Delta\mathrm{Hb}(t)$ was observed followed by a return to baseline. At 0.5 cm^3 of occlusion, another increase in $\Delta\mathrm{Hb}(t)$ was observed. At 0.6 cm^3 occlusion, the fetal $\Delta\mathrm{Hb}(t)$ rose above baseline. At 0.7 cm^3 of occlusion, there was a steep rise in $\Delta\mathrm{Hb}(t)$ and a decrease in $\Delta\mathrm{HbO}(t)$. At this point the fetal SaO_2 was measured to be close to 10% and the catheterized balloon was completely drained of all the saline. A return to baseline was immediately noticeable in both the $\Delta\mathrm{HbO}(t)$ and $\Delta\mathrm{Hb}(t)$ traces. The fetus needed approximately 8 min to fully recover (Fig. 1).

At the start of the second trial, at 0.3 cm^3 of occlusion there was again a slight jump in $\Delta\mathrm{Hb}(t)$ followed by a return to baseline. At 0.5 cm^3 of occlusion, there was again an increase in $\Delta\mathrm{Hb}(t)$. At 0.6 cm^3 of occlusion, there was a sharp increase in $\Delta\mathrm{Hb}(t)$ from baseline with an accompanying decrease in $\Delta\mathrm{HbO}(t)$. At this point, the fetal SaO_2 was again measured to be close to 10%. In this second trial, instead of completely draining the balloon of saline, the volume of occlusion was decremented in a step-wise fashion. As occlusion was brought down to a volume of 0.4 cm^3, the $\Delta\mathrm{Hb}(t)$ fell, while the $\Delta\mathrm{HbO}(t)$ fluctuated below baseline. As the volume

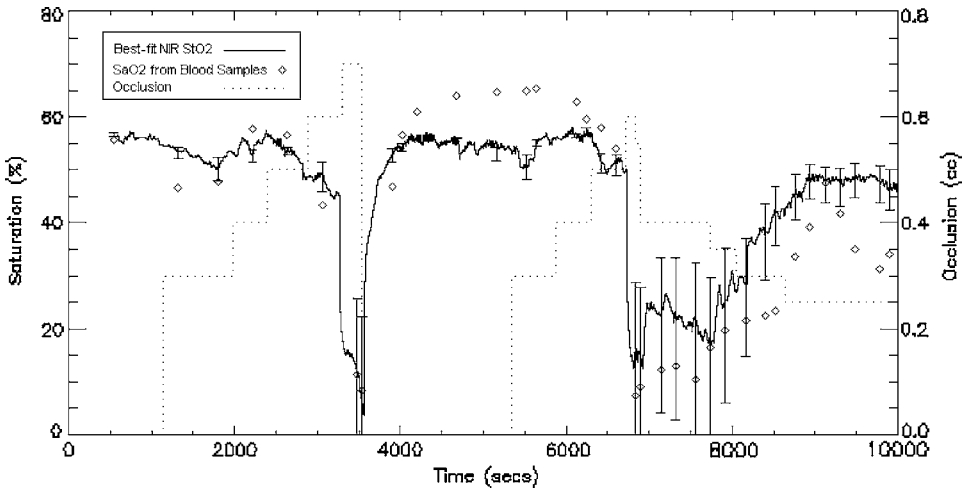

Fig. 2 Fetal StO_2 calculated from NIR measurements. The diamonds represent the fetal SaO_2 measurements taken from blood gas analysis. The solid line is the average $StO_2(t)$ trace calculated the NIR data using the analytical semi-infinite model. The dotted line represents the volume of occlusion. The error bars represent the maximum variations in the calculated fetal StO_2 as a result of altering all of the parameters in Table 1 simultaneously.

of occlusion was reduced to 0.35 cm^3, the $\Delta HbO(t)$ began a more rapid return to baseline. At 0.3 cm^3 of occlusion, the $\Delta Hb(t)$ also began a prompt return to baseline (Fig. 2). The ultrasound fetal heart rate monitor verified that the fetus remained alive throughout the entire experiment.

The calculated NIR $StO_2(t)$ curve also demonstrates a direct hemodynamic response due to the induced occlusion (Fig. 2). In the first hypoxic cycle, as the catheterized balloon reached a volume of 0.7 cm^3, the fetal tissue blood saturation dropped sharply. In the second cycle, hypoxia was induced at an occlusion volume of 0.6 cm^3. As the saline was withdrawn from the balloon, the NIR StO_2 measurements returned to the tissue blood saturation baseline.

However, the SaO_2 measurements overshoot the NIR StO_2 measurements after the first recovery and undershoot the NIR StO_2 measurements during the second recovery (Fig. 2). Figure 3 shows how the calculated StO_2 correlates to the SaO_2 measurements. The relationship is not strongly linear over the whole range of SaO_2 measurements. However, without any fetal venous blood saturation measurements, it is unknown whether the calculated StO_2 is linear with some weighted average of SaO_2 and SvO_2. This weighted average may have also fluctuated during the experiment.[40]

3.2 *Error Propagation in* $StO_2(t)$

The NIR StO_2 results were obviously most reliable while fetal oxygenation remained in close proximity to the fetal status at baseline. However, as fetal hypoxia was induced and fetal saturation levels fell, uncertainty in any of the assumed baseline parameters resulted in more variability in the calculated NIR StO_2 measurements.

In this study, the global reduced scattering coefficient, the baseline maternal absorption coefficient, and the baseline fetal absorption coefficient were independently varied over a range of possible values in order to investigate the error propagation in the calculated NIR StO_2 measurements. The effect of error in each of the baseline parameters on the resulting StO_2 calculation was measured as the fractional error (Fig. 3), given by:

$$\left(\frac{\Delta StO_2}{StO_2}\right) = \frac{\max(StO_2) - \min(StO_2)}{\overline{StO_2}}, \tag{19}$$

where $\max(StO_2)$ and $\min(StO_2)$ refer to the extrema of StO_2 and $\overline{StO_2}$ represents the mean StO_2 calculated at a specific point in time.

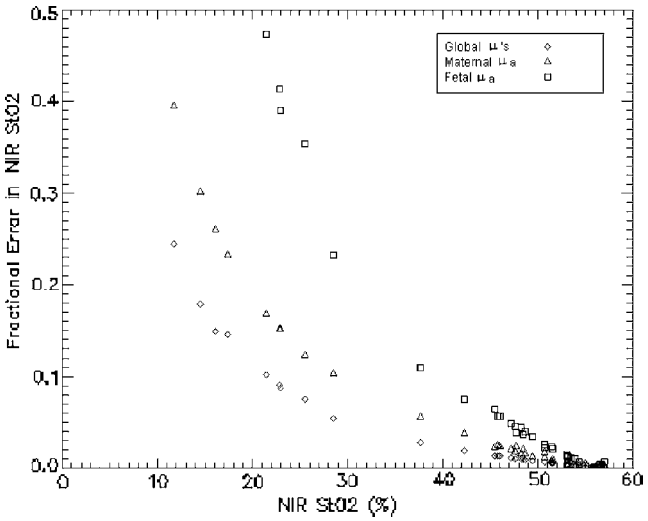

Fig. 3 Fractional error due to uncertainty in baseline optical properties. The triangles represent the fractional error in the calculated NIR StO_2 results due to altering the maternal baseline absorption coefficient (i.e., the maternal tHb and StO_2 parameters) over the specified range of reasonable values (Table 1). The squares represent the fractional error due to uncertainty in the baseline fetal absorption coefficient (in particular, the fetal tHb). The diamonds represent the fractional error due to uncertainty in μ_s'.

The results of the error analysis show that uncertainty in the global reduced scattering coefficient, the baseline maternal absorption coefficient, and the baseline fetal absorption coefficient have similar effects on the NIR calculations. The error propagation due to the baseline maternal absorption coefficient was deduced by combining the effects of both the maternal tHb and the maternal baseline StO_2. The baseline fetal absorption coefficient was analyzed by varying the fetal tHb while the baseline fetal StO_2 was held constant at the initial fetal SaO_2 reading (a likely saturation region).

Above a best-fit StO_2 of 40% (i.e., the StO_2 calculated using the best-fit baseline parameters determined from the minimization routine), the fractional errors due to uncertainty in the baseline parameters are relatively low, between 0.1 and 0.2 (Fig. 3). It has been found in several animal studies, during which fetal arterial blood gas samples were drawn, that the "normal" range of fetal SaO_2 generally falls between 30 and 80%. (Studies have shown that fetal oxygen saturation below 30% is associated with declining fetal arterial pH.[41]) Therefore, these results are optimistic that fetal imbalance would most likely be detectable by the NIR StO_2.

3.3 *Potential Sources of Error in* StO_2

Several broad assumptions were made about the baseline parameters considered in this study. First, it was assumed that the baseline parameters are restricted to a known range of values (Table 1), which was determined by values reported in the literature. However, it remains possible that these baseline values fall outside the expected range.

Second, an important parameter which has not been considered here is the baseline fetal StO_2. The variation of this parameter is equivalent to varying $StO_2(t=0)$, which essentially shifts the NIR $StO_2(t)$ curve. In this case, it was assumed that the fetal tissue blood saturation was approximately equal to the arterial saturation, and was fixed to the SaO_2 reading from the blood gas analysis. This may not always be the case, however, in an uncontrolled *in vivo* system. Knowledge of the true system geometry as well as a multidistance instrument are necessary to more accurately determine μ_{a0} (a function of both fetal and maternal tHb and StO_2), which is variable from subject to subject.

The background absorption is another parameter that could be given more consideration in a further study. Here, it was assumed that the background absorption remains constant throughout the experiment. It was also assumed to be of equal weight in both the maternal and fetal layers. In actuality, the background absorption in the fetal layer could be due to a fat or water concentration different from that in the maternal layer. These concentrations may also change with variations in blood oxygenation.[40]

It was also assumed that the scattering coefficient remained constant throughout the experiment, over all stages of hypoxia. Other investigations have shown that the scattering coefficient does vary with oxygen saturation.[40] This could lead to additional error, since any fluctuations in the data were considered solely absorptive. However, the changes in the absorption coefficient are much greater than those typically found in the scattering coefficient, so any error attributed to this assumption would most likely be relatively small.

The analytical model used to analyze the NIR data was also founded on assumptions. In order to quantify the fluctuations in the data as fetal chromophore concentration changes, it was assumed that the maternal layer experienced no fluctuations [Eq. (12)]. This assumption was based on the maternal arterial oxygen saturation values recorded by a pulse oximeter placed on the maternal ear. Yet, this does not ensure that no blood saturation changes occurred locally, in the maternal tissue visible to the source-detector probe.

The feasibility of detecting the blood oxygen saturation of the fetal head, *in utero*, has been shown here. However, there is still much work to be done in the way of perfecting an instrument that would be used and trusted in a real clinical setting. One large concern arises from the fact that there is a layer of amniotic fluid between the fetal head and the maternal layer, characterized by a low absorption coefficient and a low scattering coefficient. This layer of amniotic fluid varies in thickness depending on the gestational age of the fetus and the fetal position. It has been shown that intervening amniotic fluid can significantly affect the photon migration path directly below the source. A large fraction of photons will be diverted around the fetal head before being detected at the surface, resulting in a smaller average absorption.[22] A numerical model based on the radiative transport equation would more accurately simulate photon migration in cases where there is a nonuniform contact between the maternal abdomen and the fetal head. However, in cases of a late fetal gestational age, where the amniotic fluid layer is minimized, a simple two-layer diffusion model, such as that used in this study, will suffice.

Acknowledgments

This research was supported in part by National Institutes of Health (NIH) grant HL061057, by a NIH-supported research resource grant, P41-RR02305, and by the National Heart, Lung, and Blood Institute, T32-HL07614.

References

1. D. James, "Recent advances: fetal medicine," *Br. Med. J.* **316**, 1580–1583 (1998).
2. National Institute of Child Health, "Electronic fetal heart rate monitoring: research guidelines for interpretation," *Am. J. Obstet. Gynecol.* **177**(6), 1385–1390 (1997).
3. K. B. Nelson, J. M. Dambrosia, T. Y. Ting, and J. K. Grether, "Uncertain value of electronic fetal monitoring in predicting cerebral palsy," *N. Engl. J. Med.* **334**(10), 613–618 (1996).
4. K. W. Murphy, P. Johnson, J. Moorcraft, R. Pattinson, V. Russell, and A. Turnbull, "Birth asphyxia and the intrapartum cardiotocograph," *Br. J. Obstet. Gynaecol.* **97**(6), 470–479 (1990).
5. W. W. Hay, Jr., D. J. Rodden, S. M. Collins, D. L. Melara, K. A. Hale, and L. M. Fashaw, "Reliability of conventional and new pulse oximetry in neonatal patients," *J. Perinatol* **22**(5), 360–366 (2002).
6. B. Chance, *Photon Migration in Tissue*, Plenum, New York (1989).
7. F. F. Jobsis, "Noninvasive, infrared monitoring of cerebral and myocardial oxygen sufficiency and circulatory parameters," *Science* **198**(4323), 1264–1267 (1977).
8. P. L. Madsen and N. H. Secher, "Near-infrared oximetry of the brain," *Prog. Neurobiol.* **58**(6), 541–560 (1999).
9. B. Chance, R. Alfano, and B. Tromberg, Eds., *Optical Tomography and Spectroscopy of Tissue: Theory, Instrumentation, Model, and Human Studies II*, *Proc. SPIE* **2979** (1997).
10. A. Duncan, J. H. Meek, M. Clemence, C. E. Elwell, L. Tyszczuk, M. Cope, and D. T. Delpy, "Optical pathlength measurements on adult head, calf and forearm and the head of the newborn infant using phase resolved optical spectroscopy," *Phys. Med. Biol.* **40**(2), 295–304 (1995).

11. D. T. Delpy and M. Cope, "Quantification in tissue near-infrared spectroscopy," *Philos. Trans. R. Soc. London, Ser. B* **352**, 649–659 (1997).
12. C. D. Kurth and B. Uher, "Cerebral hemoglobin and optical pathlength influence near-infrared spectroscopy measurement of cerebral oxygen saturation," *Anesth. Analg. (Paris)* **84**(6), 1297–1305 (1997).
13. S. R. Arridge, M. Cope, and D. T. Delpy, "The theoretical basis for the determination of optical pathlengths in tissue: temporal and frequency analysis," *Phys. Med. Biol.* **37**(7), 1531–1560 (1992).
14. E. M. Sevick, B. Chance, J. Leigh, S. Nioka, and M. Maris, "Quantitation of time- and frequency-resolved optical spectra for the determination of tissue oxygenation," *Anal. Biochem.* **195**(2), 330–351 (1991).
15. J. C. Hebden, A. Gibson, R. M. Yusof, N. Everdell, E. M. Hillman, D. T. Delpy, S. R. Arridge, T. Austin, J. H. Meek, and J. S. Wyatt, "Three-dimensional optical tomography of the premature infant brain," *Phys. Med. Biol.* **47**(23), 4155–4166 (2002).
16. Y. Hoshi, "Functional near-infrared optical imaging: utility and limitations in human brain mapping," *Psychophysiology* **40**(4), 511–520 (2003).
17. E. Keller, A. Nadler, H. Alkadhi, S. S. Kollias, Y. Yonekawa, and P. Niederer, "Noninvasive measurement of regional cerebral blood flow and regional cerebral blood volume by near-infrared spectroscopy and indocyanine green dye dilution," *Neuroimage* **20**(2), 828–839 (2003).
18. S. L. Jacques, N. Ramanujam, G. Vishnoi, R. Choe, and B. Chance, "Modeling photon transport in transabdominal fetal oximetry," *J. Biomed. Opt.* **5**(3), 277–282 (2000).
19. N. Ramanujam, H. Long, M. Rode, I. Forouzan, M. Morgan, and B. Chance, "Antepartum, transabdominal near infrared spectroscopy: feasibility of measuring photon migration through the fetal head in utero," *J. Matern.-Fetal Med.* **8**(6), 275–288 (1999).
20. A. Zourabian, A. Siegel, B. Chance, N. Ramanujan, M. Rode, and D. A. Boas, "Transabdominal monitoring of fetal arterial blood oxygenation using pulse oximetry," *J. Biomed. Opt.* **5**(4), 391–405 (2000).
21. S. J. Matcher, "Performance comparison of several published tissue near-infrared spectroscopy algorithms," *Anal. Biochem.* **227**, 54–68 (1995).
22. G. Vishnoi, A. H. Hielscher, N. Ramanujam, and B. Chance, "Photon migration through fetal head in utero using continuous wave, near-infrared spectroscopy: development and evaluation of experimental and numerical models," *J. Biomed. Opt.* **5**(2), 163–172 (2000).
23. B. W. Pogue, K. D. Paulsen, C. Abele, and H. Kaufman, "Calibration of near-infrared frequency-domain tissue spectroscopy for absolute absorption coefficient quantitation in neonatal head-simulating phantoms," *J. Biomed. Opt.* **5**(2), 185–193 (2000).
24. N. Ramanujam, G. Vishnoi, A. Hielscher, M. Rode, I. Forouzan, and B. Chance, "Photon migration through fetal head in utero using continuous wave, near infrared spectroscopy: clinical and experimental model studies," *J. Biomed. Opt.* **5**(2), 173–184 (2000).
25. R. Choe, T. Durduran, G. Yu, M. J. Nijland, B. Chance, A. G. Yodh, and N. Ramanujam, "Transabdominal near infrared oximetry of hypoxic stress in fetal sheep brain in utero," *Proc. Natl. Acad. Sci. U.S.A.* **100**(22), 12950–12954 (2003).
26. M. J. Nijland, U. Shankar, V. Iyer, and M. G. Ross, "Assessment of fetal scalp oxygen saturation determination in the sheep by transmission pulse oximetry," *Am. J. Obstet. Gynecol.* **183**(6), 1549–1553 (2000).
27. B. Chance and R. R. Alfano, Eds., *Optical Tomography, Photon Migration, and Spectroscopy of Tissue and Model Media: Theory, Human Studies, and Instrumentation, Parts 1 and 2*, *Proc. SPIE* **2389** (1995).
28. A. Ishimaru, *Wave Propagation and Scattering in Random Media*, Academic Press, New York (1978).
29. T. Nakai, G. Nishimura, and K. Yamamoto, "Expression of optical diffusion coefficient in high-absorption turbid media," *Electron. Commun. Jpn., Part 2: Electron.* part 2, **81**(11), 34–41 (1998).
30. R. C. Haskell, L. O. Svaasand, T. T. Tsay, T. C. Feng, M. S. McAdams, and B. J. Tromberg, "Boundary conditions for the diffusion equation in radiative transfer," *J. Opt. Soc. Am. A* **11**(10), 2727–2741 (1994).
31. T. J. Farrell, M. S. Patterson, and B. Wilson, "A diffusion theory model of spatially resolved, steady-state diffuse reflectance for the noninvasive determination of tissue optical properties in vivo," *Med. Phys.* **19**(4), 879–888 (1992).
32. A. Kienle and M. S. Patterson, "Improved solutions of the steady-state and the time-resolved diffusion equations for reflectance from a semi-infinite turbid medium," *J. Opt. Soc. Am. A* **14**(1), 246–254 (1997).
33. J. S. Souris, "Diffusing wave emission tomography in highly-scattering systems: a dissertation in biochemistry and molecular biophysics," Ph.D. Thesis, University of Pennsylvania (1999).
34. M. Hiraoka, M. Firbank, M. Essenpreis, M. Cope, S. R. Arridge, P. van der Zee, and D. T. Delpy, "A Monte Carlo investigation of optical pathlength in inhomogeneous tissue and its application to near-infrared spectroscopy," *Phys. Med. Biol.* **38**(12), 1859–1876 (1993).
35. M. Cope, "The application of near infrared spectroscopy to non-invasive monitoring of cerebral oxygenation in the newborn infant," Ph.D. Thesis, University College of London (1991).
36. A. Gibson, R. M. Yusof, H. Dehghani, J. Riley, N. Everdell, R. Richards, J. C. Hebden, M. Schweiger, S. R. Arridge, and D. T. Delpy, "Optical tomography of a realistic neonatal head phantom," *Appl. Opt.* **42**(16), 3109–3116 (2003).
37. P. Taroni, A. Pifferi, A. Torricelli, D. Comelli, and R. Cubeddu, "In vivo absorption and scattering spectroscopy of biological tissues," *Photochem. Photobiol. Sci.* **2**(2), 124–129 (2003).
38. J. S. Matcher, M. Cope, and D. T. Delpy, "In vivo measurements of the wavelength dependence of tissue-scattering coefficients between 760 and 900 nm measured with time-resolved spectroscopy," *Appl. Opt.* **36**, 386–396 (1997).
39. W. H. Press and Numerical Recipes Software (Firm, *Numerical Recipes in C*, Cambridge University Press, Cambridge, England, New York (1993).
40. D. M. Hueber, M. A. Franceschini, H. Y. Ma, Q. Zhang, J. R. Ballesteros, S. Fantini, D. Wallace, V. Ntziachristos, and B. Chance, "Non-invasive and quantitative near-infrared hemoglobin spectrometry in the piglet brain during hypoxic stress, using a frequency-domain multidistance instrument," *Phys. Med. Biol.* **46**(1), 41–62 (2001).
41. D. M. Gorenberg, C. Pattillo, P. Hendi, P. J. Rumney, and T. J. Garite, "Fetal pulse oximetry: correlation between oxygen desaturation, duration, and frequency and neonatal outcomes," *Am. J. Obstet. Gynecol.* **189**(1), 136–138 (2003).